Energy, Mines and Resources Canada
Énergie, Mines et Ressources Canada

CANMET

Canada Centre for Mineral and Energy Technology
Centre canadien de la technologie des minéraux et de l'énergie

Mining Research Laboratories
Laboratoires de recherche minière

ELECTRICAL CHARGE AND PARTICLE SIZE CHARACTERISTICS OF RADON PROGENY, THORON PROGENY AND LONG-LIVED RADIOACTIVE DUST

J. BIGU ELLIOT LAKE LABORATORY

MRL 89-62(OP) MAY 1989

Canada

MRL 89-62 (OP) c.1

ELECTRICAL CHARGE AND PARTICLE SIZE CHARACTERISTICS OF RADON PROGENY, THORON PROGENY AND LONG-LIVED RADIOACTIVE DUST

J. BIGU ELLIOT LAKE LABORATORY

MRL 89-62(OP) MAY 1989

Presented to American Industrial Hygiene Conference, St. Louis, Missouri, U.S.A., May 21-26, 1989

ELECTRICAL CHARGE AND PARTICLE SIZE CHARACTERISTICS OF RADON PROGENY, THORON PROGENY AND LONG-LIVED RADIOACTIVE DUST

J. Bigu*

ABSTRACT

The electrical charge and particle size characteristics of radon (^{222}Rn) progeny, thoron (^{220}Rn) progeny, and Long-Lived Radioactive Dust (LLRD) have been determined. Radon progeny measurements were carried out in a large Radon/Thoron Test Facility (RTTF) of the walk-in type. Thoron progeny and LLRD measurements were conducted in an underground uranium mine. An electrical elutriator of the two split-flow type was used in the measurements in conjunction with a variety of aerosol and radiation instrumentation. Two mining operations were monitored, namely, a crushing operation and an ore transportation operation. The electrical charge (n) measured for the ^{222}Rn progeny and ^{220}Rn progeny was similar, namely, n ~0.45. The electrical charge for the LLRD was very dependent on the mining operation, being substantially higher for the crushing operation than for the ore transportation operation. The electrical charge varied with the particle size increasing with particle size. An electrical charge of n ~500 was measured for the crushing operation at a particle size of 8 μm. In all cases, n for the mining operation was much higher than that predicted theoretically by Boltzmann's distribution.

Key words: Electrical charge; particle size; long-lived radioactive dust; radon progeny; thoron progeny.

*Research Scientist and Radiation/Respirable Dust/Ventilation Project Leader, Elliot Lake Laboratory, CANMET, Energy, Mines and Resources Canada, Elliot Lake, Ontario, Canada.

CHARGE ÉLECTRIQUE ET TAILLE DES PARTICULES DES DESCENDANTS RADIOACTIFS DU RADON, DES DESCENDANTS RADIOACTIFS DU THORON ET DES POUSSIÈRES RADIOACTIVES À PÉRIODE LONGUE

J. Bigu*

RÉSUMÉ

Les charges électriques et les tailles des particules des descendants radioactifs du radon (^{222}Rn), des descendants radioactifs du thoron (^{220}Rn) et des poussières radioactives à période longue ont été déterminées. Les mesures concernant les descendants du radon ont été effectuées dans une grande installation de détection de radon/thoron de type chambre. Les mesures concernant les descendants du thoron et les poussières radioactives ont été réalisées dans une mine d'uranium souterraine. Pour ces mesures, nous avons utilisé conjointement un élutriateur électrique à deux courants divergents et divers instruments de mesure des aérosols et des rayonnements. Deux opérations minières ont été monitorées, à savoir une opération de broyage et une opération de transport du minerai. Les charges électriques (n) mesurées pour ^{222}Rn et pour ^{220}Rn étaient similaires, soit $n \sim 0,45$. La charge électrique des poussières radioactives à période longue était très variable suivant l'opération minière: elle était beaucoup plus élevée pour le broyage que pour le transport du minerai. La charge électrique augmentait avec la taille des particules. Nous avons mesuré une charge électrique de $n \sim 500$ lors de l'opération de broyage pour une taille de particule de 8 µm. Dans tous les cas, la valeur de n observée lors des opérations minières était beaucoup plus élevée que celle prévue théoriquement à partir de la distribution de Boltzmann.

Mots-clés: Charge électrique; taille de particule; poussière radioactive à période longue; descendant radioactif du radon; descendant radioactif du thoron

*Chercheur et chef du projet sur les rayonnements, la poussière inhalable et la ventilation, Laboratoire d'Elliot Lake, CANMET, Énergie, Mines et Ressources Canada, Elliot Lake (Ontario) Canada

INTRODUCTION

The short-lived decay products of ^{222}Rn and ^{220}Rn are initially formed in an atomic, positively charged state which rapidly combines with submicron aerosols (1-4). As aerosols are found in positively, negatively and neutrally charged states, the resulting atmosphere consists of a complex mixture of charged and neutral particles of size covering a wide range.

Similarly, measurements have shown that industrial dusts in the respirable size range also carry an electrical charge (5-9). The electrical charge associated with Long-Lived Radioactive Dust (LLRD), i.e., dust containing long-lived radioisotopes, is important from the health physics standpoint because it influences the deposition of these particles in the human respiratory system (10). Long-Lived Radioactive Dust is found in mine air in the course of mining operations in uranium mines. Rn-222 and ^{220}Rn progeny are also found in uranium mines. These two radioactive gases are formed, respectively, in the decay of ^{226}Ra and ^{224}Ra, radioisotopes which are found in uranium ores contained in mine walls. Rn-222 and ^{220}Rn find their way from mine walls into mine openings by diffusion and transport mechanisms.

Because of the electrical charge associated with the ^{222}Rn and ^{220}Rn progeny and with LLRD, these radioactive particles can be influenced by external electric and magnetic fields (11-14), thereby providing a means to reduce radiation levels in working areas.

The electrical characteristics of radioactive and non-radioactive aerosols, and industrial dusts, have been investigated by several workers (1,8,9,13-19). This paper deals with the electrical characteristics of: a) ^{220}Rn progeny in underground uranium mine atmospheres; b) LLRD generated in the course of several mining operations in an underground uranium mine; c) ^{222}Rn progeny atmospheres produced in a Radon/Thoron Test Facility (RTTF) of

the walk-in type.

An electrical elutriator of the two split-flow type, designed by Johnston (20), in conjunction with a variety of radioactivity and aerosol measuring instrumentation, has been used in this study.

DESCRIPTION OF THE ELECTRICAL ELUTRIATOR

The electrical elutriator, heretofore commonly referred to as the Split-Flow Elutriator, or SFE for short, basically consists of two halves that make up the main body of the elutriator, a flow-splitting end cap and two stainless steel parallel plates to which a variable voltage can be applied. The main body and the flow-splitting assembly are made from high-resistivity laminated epoxy resin sheets.

The elutriator channel, lined with the steel plates, is 35 cm in length, 8.6 cm in width, and 0.8 cm in height.

The size of the SFE channel was designed to operate at a nominal flowrate of 3 L min^{-1}. This flowrate permits laminar flow conditions in the channel and provides an air clearance time of less than 5 sec.

The particular design of the flow-splitting assembly allows the SFE to be used under two different modes of operation of practical interest, namely:

1. Determination of the charge distribution of the aerosol or dust cloud without polarity discrimination: hereafter referred to as configuration X.
2. Determination of aerosol or dust cloud charge distribution with polarity discrimination, i.e., both polarities are simultaneously measured; hereafter referred to as configuration Y.

In the first case (configuration X), all sampling ports in the flow-splitting assembly are connected together and counted by means of, say, an optical particle counter (OPC) for dust, or a condensation nuclei counter (CNC), for aerosols.

In the second case (configuration Y), the sampling ports in the flow-splitting assembly of the SFE are connected to two different aerosol or dust concentration monitors, or any similar arrangement for some specific purpose other than that described in this paper.

The reader is advised to consult references 8, 9 and 20 for a more detailed description of the SFE and of its applications in dust work. It should also be noted that the term aerosol and dust are used here in their more general sense to indicate radioactive (e.g., ^{222}Rn and ^{220}Rn progeny) and non-radioactive aerosols, and radioactive (e.g., LLRD) and non-radioactive dust in the respirable size range.

OTHER APPARATUSES USED

Dust and LLRD concentration and size distribution measurements were conducted using an 8-stage cascade impactor (Sierra Model 210, distributed by Andersen, U.S.A.) operated at a flowrate of 10 L min^{-1}. This instrument also provided Mass Median Aerodynamic Diameter (MMAD) and Activity Median Aerodynamic Diameter (AMAD) data. In addition, LLRD gross α-particle activity was measured on the substrates of the cascade impactor using conventional instrumentation. Independent, but concurrent, measurements of dust mass were made, in addition, by means of a continuous dust optical monitor (Model MiniRam PDM-3, manufactured by GCA Corporation, U.S.A.). Furthermore, and in conjunction with SFE measurements, dust particle concentration and particle size distribution were determined using 6-size range optical particle counters (OPC) (Modified HIAC/ROYCO Model 4100, manufactured by Mono Research Laboratories, Canada). These particle counters can determine dust particle concentration in six different particle size ranges simultaneously, namely, 0.5 to 1.5 μm, 1.5 to 2.0 μm, 2.0 to 3.5 μm, 3.5 to 5.0 μm, 5 to 10 μm, and >10 μm.

Submicron aerosol concentration was measured by means of a condensation nuclei counter (CNC) Model 3020, manufactured by TSI (U.S.A.). Aerosol size distribution was determined using a Differential Mobility Particle Sizer (DMPS) Model 3071 (also manufactured by TSI) in conjunction with the CNC.

THEORETICAL BACKGROUND

It can be shown that the number of elementary charges, n, on a particle is given by (20,21):

$$n = 3\pi\mu\eta\ D_P/eC \qquad \text{Eq 1}$$

where, η is the air viscosity

D_P is the particle diameter

μ is the particle mobility

e is the electron charge

C is the Cunningham slip correction (~1)

The mobility of the particle can be obtained from the flowrate conditions and the physical dimensions of the SFE as follows (20,21):

$$\mu = F(Q/V_o) \qquad \text{Eq 2}$$

where, Q is the sampling flowrate ($m^3\ s^{-1}$)

F is a geometrical factor given by b/wl, where, b, w and l are the physical dimensions of the SFE (i.e., w and l, are, respectively, the channel width and the channel length, whereas b is half the SFE channel height. All dimensions in m).

V_o is a voltage defined as follows: particle concentration data are tabulated as a function of voltage differential applied to the SFE. The data are then normalized to zero volt concentration and plotted. A tangent passing through the 50% normalized concentration point defines the voltage V_o by drawing a vertical line to the x-axis (i.e., voltage) from tangent contact point.

Substituting Equation 2 into Equation 1, one gets the number of elementary charges on a particle of size D_P:

$$n = 3\pi\ F\ K(D_P/V_o) \qquad \text{Eq 3}$$

where,

$$K = \eta\ Q/eC \qquad \text{Eq 4}$$

Taking into account that for the SFE used here, $w = 8.6 \times 10^{-2}$ m, $l = 0.35$ m, and $b = 4 \times 10^{-3}$ m, it can be shown that Equation 3 reduces to:

$$n = 7.036 \times 10^{9}\ (D_P/V_o) \qquad \text{Eq 5}$$

where D_P is in meters.

The procedure outlined above (21) can be applied to particles of different sizes in a dust or aerosol cloud in order to obtain the electrical charge distribution of the cloud. This procedure is straightforward for clouds with symmetric charge distributions. For clouds with asymmetric charge distributions, however, the procedure is more complex as described by Johnston elsewhere (21).

EXPERIMENTAL MEASUREMENTS AND PROCEDURES

The electric charge of aerosols in the submicron size range and LLRD in the respirable size range (~1-10 μm) have been measured.

Electrical charge characterization measurements of submicron aerosols, namely, 'total' aerosol and radioactive aerosol (^{222}Rn progeny) were carried out in a large Radon/Thoron Test Facility (RTTF) of the walk-in type. Radon gas and a mixture of NaCl aerosols and air were injected into the RTTF under turbulent flow conditions using a mixing fan for adequate mixing.

The electrical charge of LLRD and ^{220}Rn progeny was determined in an underground uranium mine. Measurements were made during a rock crushing operation at a crusher plant and during the ore transportation operation by a conveyor belt which transported the crushed material to another section of the mine for further processing.

The measurements reported in this paper were carried out using configuration X. The arrangement in Figure 1 was used to measure the electrical charge of total aerosol and ^{222}Rn progeny in the RTTF. Figure 2 was used to determine the electrical charge of LLRD.

The experimental arrangement shown in Figure 1 enabled determination of the electrical charge of total aerosol using the right hand side arm (i.e., CNC or CNC/DMPS arrangement), or the electrical charge of the radioactive aerosol using the left hand side arm of the arrangement. In the latter case, the ^{222}Rn progeny was collected in a filter/filter holder (F/FH) unit by means of a sampling pump (P) operated at 2.7 L min^{-1}. Airflow rate was measured by means of a rotameter (R). The α-particle activity collected in the filter, after a given sampling period, was measured by gross α-counting and by α-particle spectrometry using conventional instrumentation, namely α-particle scalers and an α-particle spectrometer. The experimental configuration shown in Figure 1 permitted parallel determination of the electrical charge of the ^{222}Rn progeny and of total aerosol.

The experimental arrangement shown in Figure 2 was used to determine the electrical charge of LLRD in the underground uranium mine. The electrical charge of the ^{220}Rn progeny in the mine was determined using the configuration shown in Figure 2, but substituting the OPC by the left hand side arm of Figure 1, i.e., filter/filter holder, rotameter and pump.

Measurements of particle concentration and α-particle activity were normalized and plotted versus the voltage (HV) applied to the parallel plates of the SFE. The data were analyzed using Equation 5 and the graphical procedure outlined in reference 20.

EXPERIMENTAL RESULTS

For simplicity, RTTF data and underground uranium mine data will be

presented separately.

1. RADON PROGENY AND TOTAL AEROSOL DATA IN THE RTTF

Figure 3 shows the total aerosol size distribution in the RTTF. The graph shows that the size geometric mean (G.M.) was 0.094 μm. The aerosol size range was approximately from 0.02 μm to 0.5 μm.

Figure 4 shows the normalized total aerosol concentration (upper graph) and the normalized α-particle count (lower graph) versus high voltage (H.V.) on the SFE. Using reference 20 and Equation 5, the electrical charge n for the total aerosol and the ^{222}Rn progeny is n ~0.2 and n ~0.45, respectively.

Figure 5 shows α-particle spectra (^{218}Po and ^{214}Po) from the filters for three different voltages (H.V.) on the SFE, namely, 0 V, -500 V, and -2000 V.

2. THORON PROGENY AND LLRD IN URANIUM MINE

Figure 6 shows the normalized ^{220}Rn progeny activity, i.e., ^{220}Rn progeny α-particle count, versus SFE's voltage (H.V.). Using Equation 5 and reference 20, the electrical charge can be calculated as n ~0.45. The AMAD corresponding to ^{220}Rn progeny can be calculated from Figure 9, i.e., ~0.2 μm.

Figures 7 and 8 show typical dust size concentrations, in different ranges, for the conveyor belt (Figure 7) and the crusher (Figure 8). The concentration profiles shown also include rest periods, i.e., times during which the conveyor belt carries no ore or the crusher is not in operation. The lower concentrations correspond to rest periods.

Figure 9 shows particle or activity size distribution. The graphs show LLRD percentage cumulative α-particle activity versus Equivalent Aerodynamic Diameter (EAD), graphs labelled (LLRD); LLRD percentage cumulative dust mass versus EAD (Total Dust); and ^{220}Rn progeny percentage cumulative α-particle activity versus EAD (TnD). From the above graphs it is possible to estimate the AMAD and MMAD for LLRD, and the AMAD for the ^{220}Rn progeny. The results

of several experiments are summarized below:

AMAD (LLRD) = 3.0 to 6.0 μm

AMAD (^{220}Rn progeny) = 0.2 to 0.3 μm

MMAD (LLRD) = 2.0 to 3.4 μm

Figure 10 shows the normalized LLRD particle concentration versus the voltage (H.V.) on the SFE for two different size ranges for the crusher.

Figure 11 shows the number of elementary charges (n), i.e., electrical charge of the LLRD for the two mining operations monitored, namely the conveyor belt and the crusher. Also shown is the charge expected on theoretical grounds according to Boltzmann's distribution. Figure 11 was plotted by using graphs similar to those shown in Figure 10 and calculating the electrical charge (n) according to Equation 5.

DISCUSSION OF RESULTS

The results shown in Figure 4 suggest that under our experimental conditions, ^{222}Rn progeny carried an electrical charge ~2.5 times larger than total aerosol. This result can be partly understood because: a) recently formed ^{222}Rn progeny are electrically charged and attach themselves readily to aerosols in the RTTF to form combined (i.e., attached) radioactive aerosols; and b) self-charging of attached radioactive aerosols caused by radioactive decay of ^{222}Rn progeny (22). Furthermore, because the electrical charge carried by ^{222}Rn progeny must be either 0 or an integer, $n < 1$ indicates that a fraction of the ^{222}Rn progeny cloud carries no electrical charge. From Figure 4 it can be seen that about 65% of the ^{222}Rn progeny are either positively or negatively charged whereas the remaining fraction (~35%) is in a neutrally charged state. These data are consistent with other measurements by the author et al. (13,14).

Figure 5 shows radon progeny spectra at three different voltages,

namely, 0 V, -500 V, and -2000 V. The spectra show a decrease of the ^{218}Po and ^{214}Po photopeaks with increasing H.V. No significant spectral differences as measured by the ratio $^{218}Po/^{214}Po$ were found.

Hence, from Figures 4 and 5 one may tentatively surmise the following:

1. The electrical charge on radon progeny appears to be significantly larger than that corresponding to the total aerosol cloud;
2. Both ^{218}Po and ^{214}Po are electrically charged;
3. About 65% of the radon progeny are electrically charged, either positively or negatively.

The results obtained for the ^{220}Rn progeny in the underground uranium mine were very similar to those obtained for the ^{222}Rn progeny in the RTTF. namely, the electrical charge was n ~0.45 (see Figure 6), although the AMAD corresponding to the ^{220}Rn progeny was significantly larger (0.2 to 0.3 μm) than the geometric mean particle size measured for the ^{222}Rn progeny in the RTTF (i.e., G.M. ~0.1 μm). This size difference can be understood because of: a) the presence, underground, of mineral dust particles and diesel particulates (see Figures 7 and 8); and b) size selective attachment of ^{220}Rn progeny to airborne particles. It is not clear, however, why the electrical charge should be the same under such widely different experimental conditions. This is the subject of further investigation.

The data of Figure 11 for LLRD can be represented by the analytical function:

$$n = K\, D_P^{\,m} \qquad \text{Eq 6}$$

where, K and m are numerical coefficients. Analysis of the data of Figure 11 gives the following values for this coefficient: K = 1.91 and m = 1.55 for the conveyor belt, and K = 2.1 and m = 2.83 for the crushing operation. (It should be noted that the D_P values plotted in Figure 11 correspond to the middle points of each particle size range of the OPC. Hence, the lines drawn in this

Figure do not necessarily represent the best fitting curves.)

Figure 11 shows a substantial difference in the electrical charge of dust for a given D_p for the two mining operations, namely, during the crushing operation, the value of n near the crusher was significantly higher than at the conveyor belt. The differences observed depend partly on the method of dust generation, and as discussed elsewhere (23), on self-charging effects, charge neutralization, electron transfer, ionic charge acquisition, and α-recoil mechanisms. The overall (net) effect of the dust production method, and charging, neutralization and other mechanisms on the production of electrical charge in dust particles is a function of the dust cloud residence time, whereby residence time is understood to be the time elapsed between the production of the dust cloud and its measurement. The dust cloud residence time depends on the pathway(s) followed by the cloud.

Figure 11 also shows that electrical charge (n) for the two mining operations was substantially higher than that predicted theoretically by Boltzmann's distribution (curve B.D.). The reasons for this have been dealt with in some detail elsewhere (23). Finally, as predicted theoretically, n increases with increasing particle size.

CONCLUSIONS

The average electrical charge for ^{222}Rn progeny in the RTTF and ^{220}Rn in an underground uranium mine was similar, namely, n ~2.5, and significantly higher than that for 'total' aerosol (n ~0.2) in the submicron size range (G.M. ~0.1 μm). Furthermore, about 65% of the radioactive aerosol was electrically charged.

The LLRD electrical charge for the conveyor belt operation was n ~2 at 1 μm and n ~50 at 8 μm. For the crusher, the following values were obtained: n ~3 at 1 μm and n ~500 at 8 μm. These values are much higher than those

predicted by Boltzmann's distribution.

The electrical charge on airborne particulate matter increased with increasing particle size, as anticipated on theoretical grounds.

REFERENCES

1. Porstendörfer, J. and Mercer, T.T., "Influence of electric charge and humidity upon the diffusion coefficient of radon decay products"; Health Phys. 37:191-199; 1979.

2. Dua, S.K., Kotrappa, P. and Gupta, P.C., "Influence of relative humidity on the charged fraction of decay products of radon and thoron"; Health Phys. 45:152-156; 1983.

3. Szucs, S. and Delfosse, J.M., "Charge spectrum of recoiling ^{216}Po in the α-decay of ^{220}Rn"; Phys. Rev. Letters 15:163-165; 1965.

4. Wellisch, E.M., Philos. Mag. 26:623-635; 1913.

5. Patterson, H.S., Whytlaw-Gray, R. and Cawood, W., "The structure and electrification of smoke particles"; Proc. Roy. Soc. A 124:523-532; 1929.

6. Kunkel, W.B., "The static electrification of dust particles on dispersion into a cloud"; J. Appl. Phys. 21:820-832; 1950.

7. Kunkel, W.B., "Charge distribution in coarse aerosols as a function of time"; J. Appl. Phys. 21:833-837; 1950.

8. Johnston, A.M., Vincent, J.H. and Jones, A.D., "Measurements of electric charge for workplace aerosols"; Ann. Occup. Hyg. 29:271-284; 1985.

9. Johnston, A.M., Vincent, J.H. and Jones, A.D., "Electrical charge characteristics of dry aerosols produced by a number of laboratory mechanical dispensers"; Aerosol Sci. and Tech. 6:115-127; 1987.

10. Prodi, V. and Mularoni, A., "Electrostatic lung deposition experiments

with humans and animals"; Ann. Occup. Hyg. 29:229-240; 1985.

11. Fuchs, N.A., "The Mechanics of Aerosols"; The MacMillan Company, New York, 1964.

12. Jonassen, N., "The effect of electric fields on ^{222}Rn daughter products in indoor air"; Health Phys. 45:487-491; 1983.

13. Bigu, J., "Effects of electric fields on ^{220}Rn progeny concentration"; Health Phys. 49:512-516; 1985.

14. Bigu, J. and Grenier, M., "Electrical characteristics of the short-lived decay products of thoron in underground uranium mines"; Am. Ind. Hyg. Assoc. J. 47:308-311; 1986.

15. Hoppel, W.,"Ion-aerosol attachment coefficients, ion depletion, and the charge distribution on aerosols"; J. Geophys. Res. 90:5917-5923; 1985.

16. Billard, F. and Madelaine. G., "Etude de la charge electrique portée par les aerosols"; in: Assessment of Airborne Radioactivity. Proc. of Symp. held in The International Atomic Energy Agency (IAEA) Vienna: EAEA-SM-95/13; 325-333; 1967.

17. Bricard, J., Renoux, A., Pradel, J. and Madelaine, G., "Spectre des aerosols naturels radioactifs": in: La Pollution Radioactive des Milieux Gazeux: 15-17.

18. Dus, S.K., Kotrappa, P. and Bhanti, D.P., "Electrostatic charge on decay products of thoron"; Am. Ind. Hyg. Assoc. J. 39:339-345; 1978.

19. Dua, S.K. and Kotrappa, P., "Comment on the charge on decay products of thoron and radon"; Am. Ind. Hyg. Assoc. J. 42:242-243; 1981.

20. Johnston, A.M., "A semi-automatic method for the assessment of electric charge carried by airborne dust"; J. Aerosol Sci. 14:643-655; 1983.

21. Hochrainer, D., "Measurement methods for electric charges on aerosols";

Ann. Occup. Hyg. Assoc. J. 29:241-249; 1985.

22. Yeh, H., "A theoretical study of electrical discharging of self-charging aerosols"; J. Aerosol Sci. 7:343-349; 1976.

23. Bigu, J., "Electrical charge characteristics of long-lived radioactive dust in underground uranium mine operations"; Division Report MRL 88-143(TR), CANMET, Energy, Mines and Resources Canada, 1988.

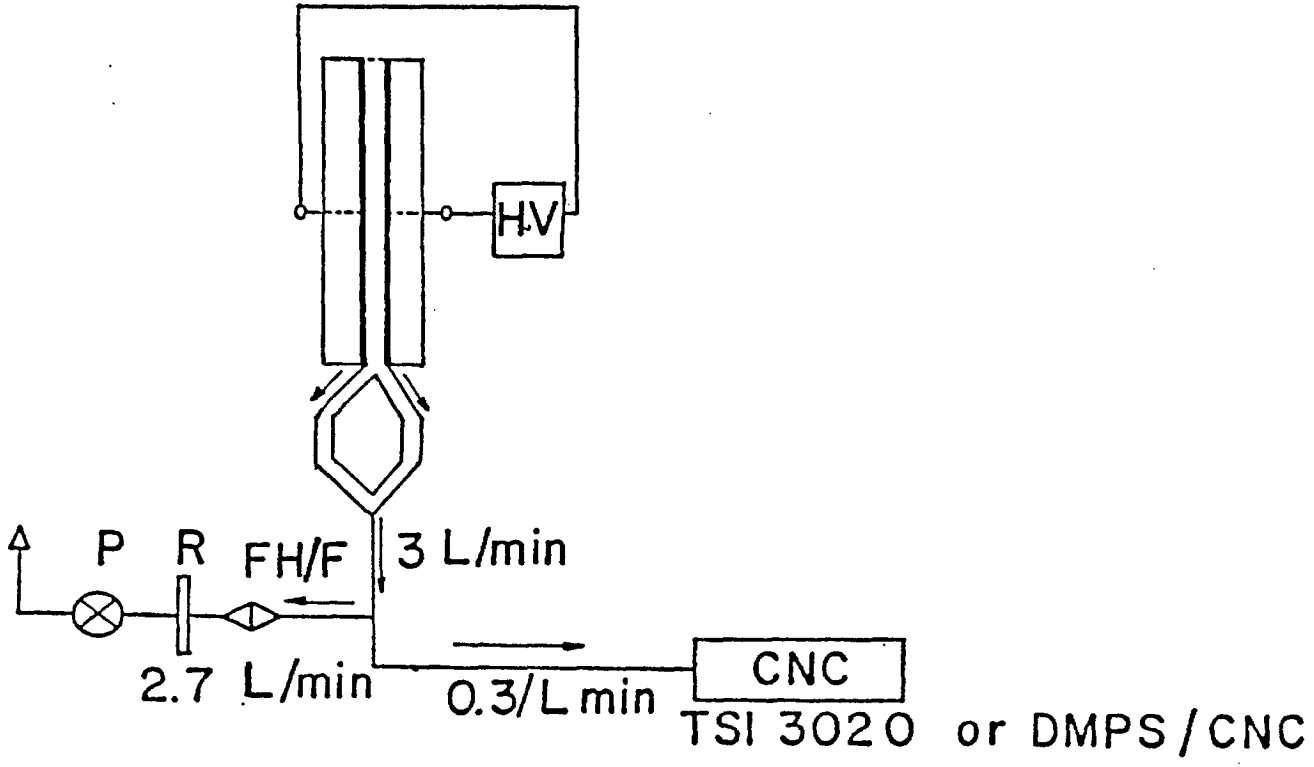

Fig. 1 - Experimental arrangement used to measure the electrical charge of total aerosol and ^{222}Rn progeny in the RTTF.

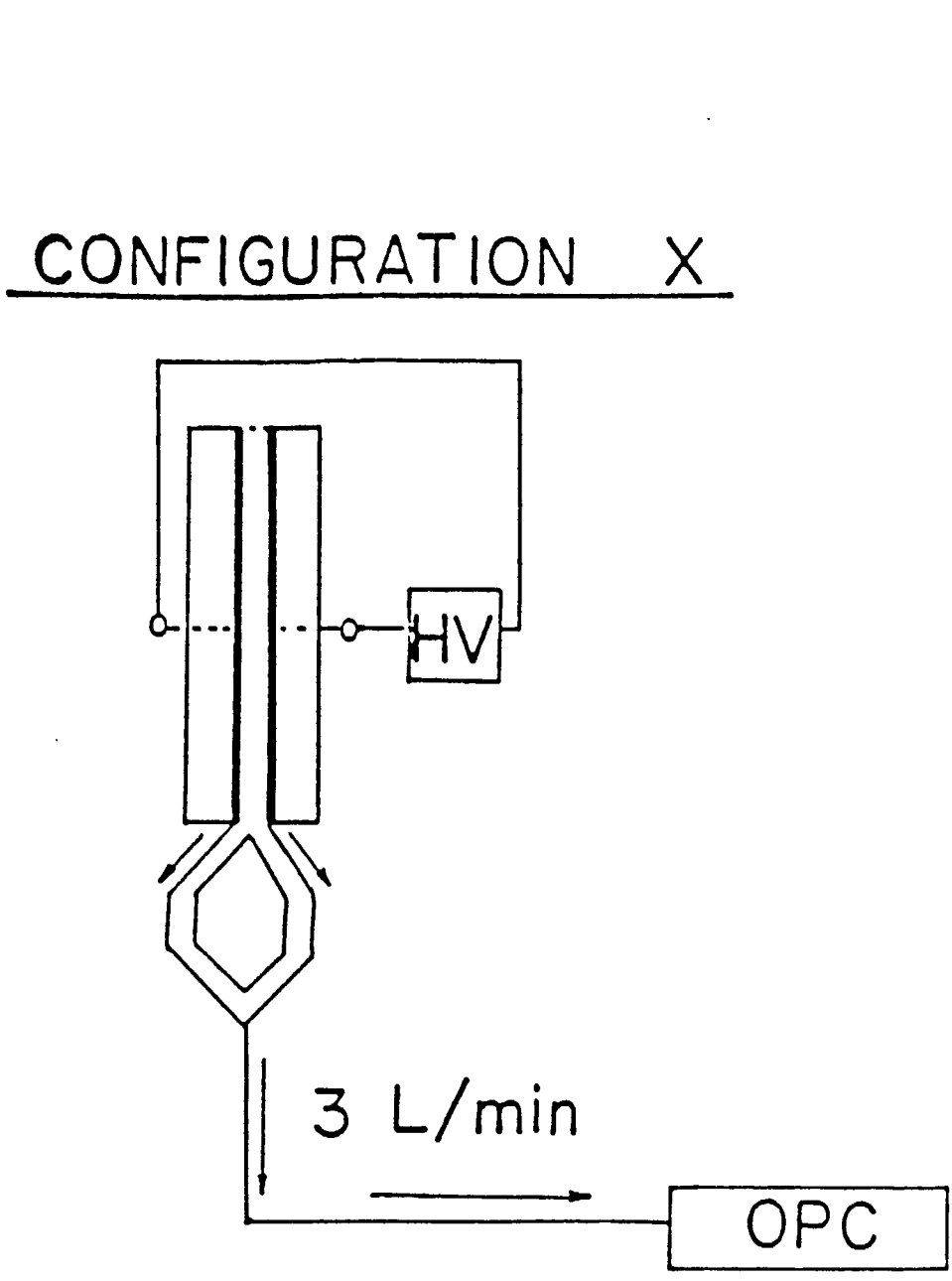

Fig. 2 - Experimental arrangement used to determine the electrical charge of LLRD.

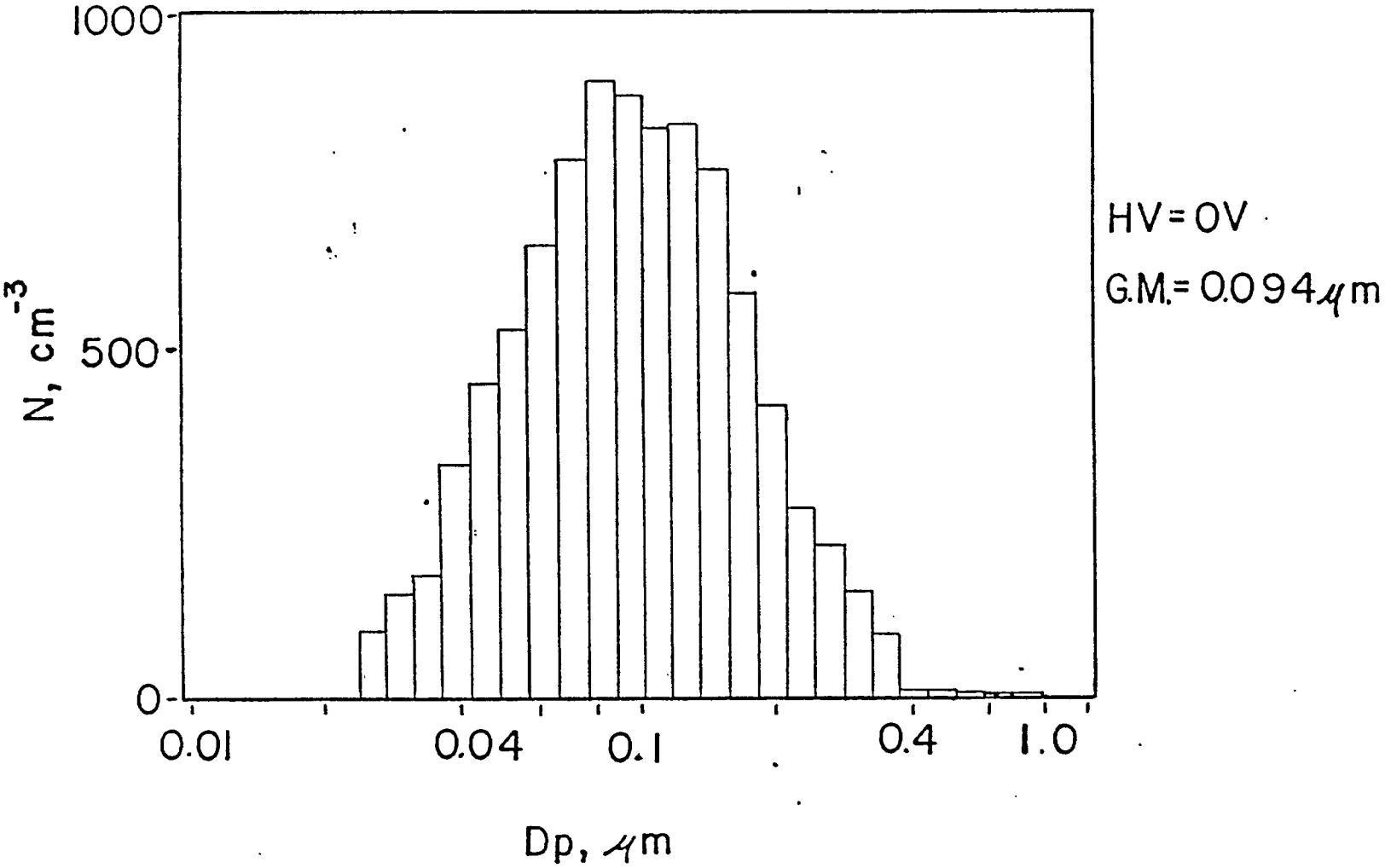

Fig. 3 - Total aerosol size distribution in the RTTF.

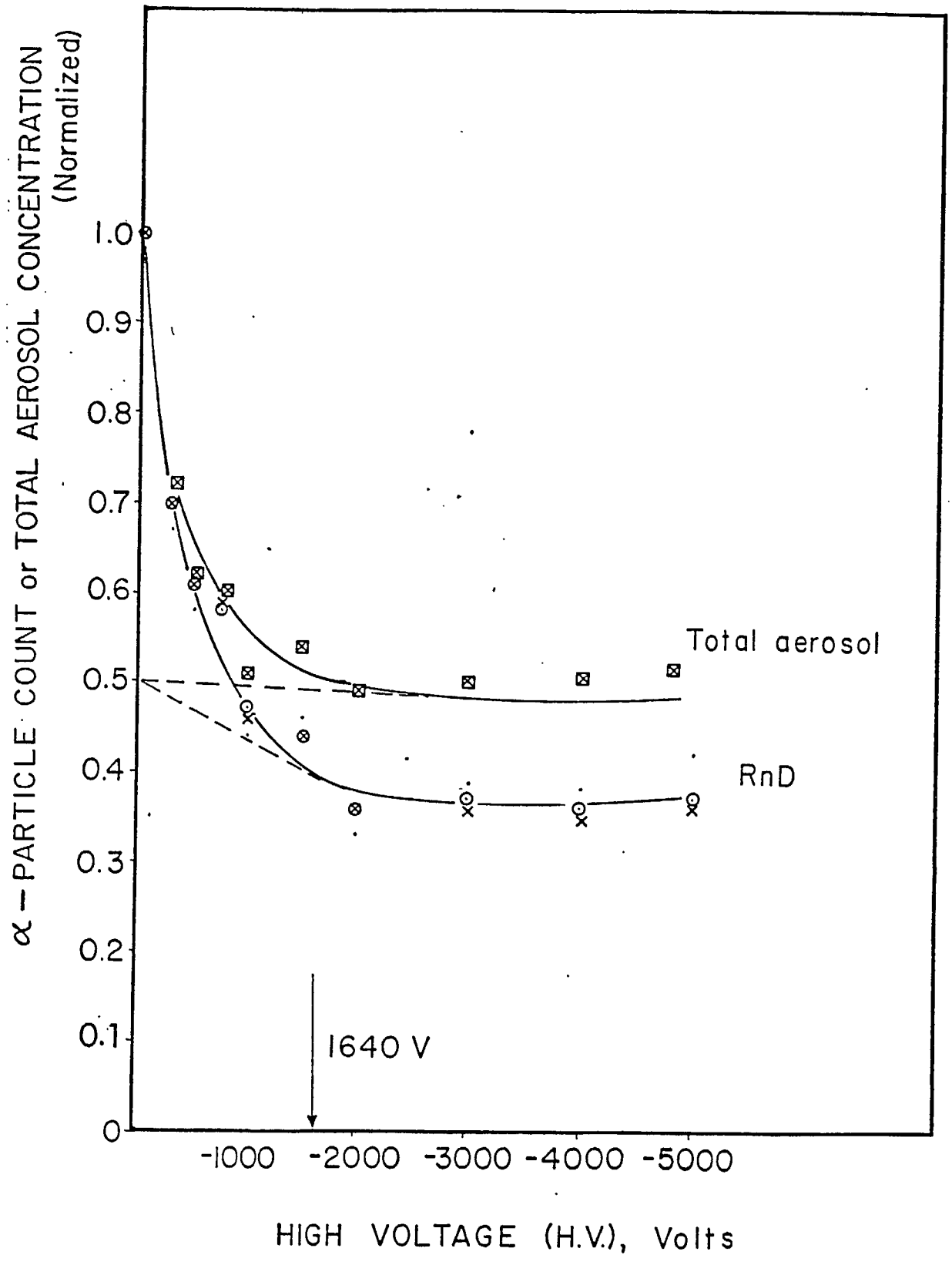

Fig. 4 - Normalized total aerosol concentration (upper graph), and normalized ^{222}Rn progeny α-particle count (lower graph) versus H.V. on the SFE.

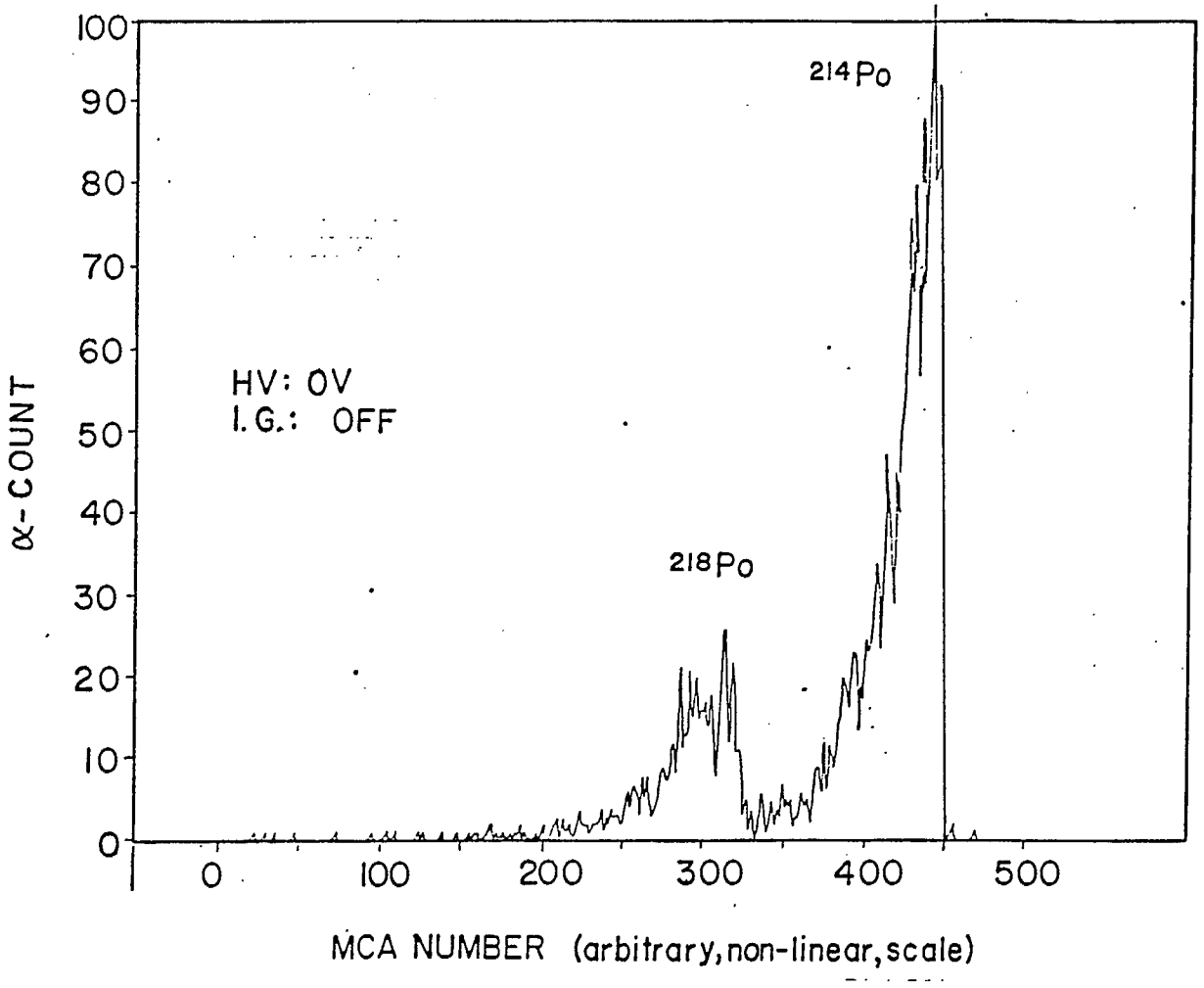

Fig. 5a - ^{222}Rn progeny spectrum (RTTF) for H.V. = 0 V on the SFE.

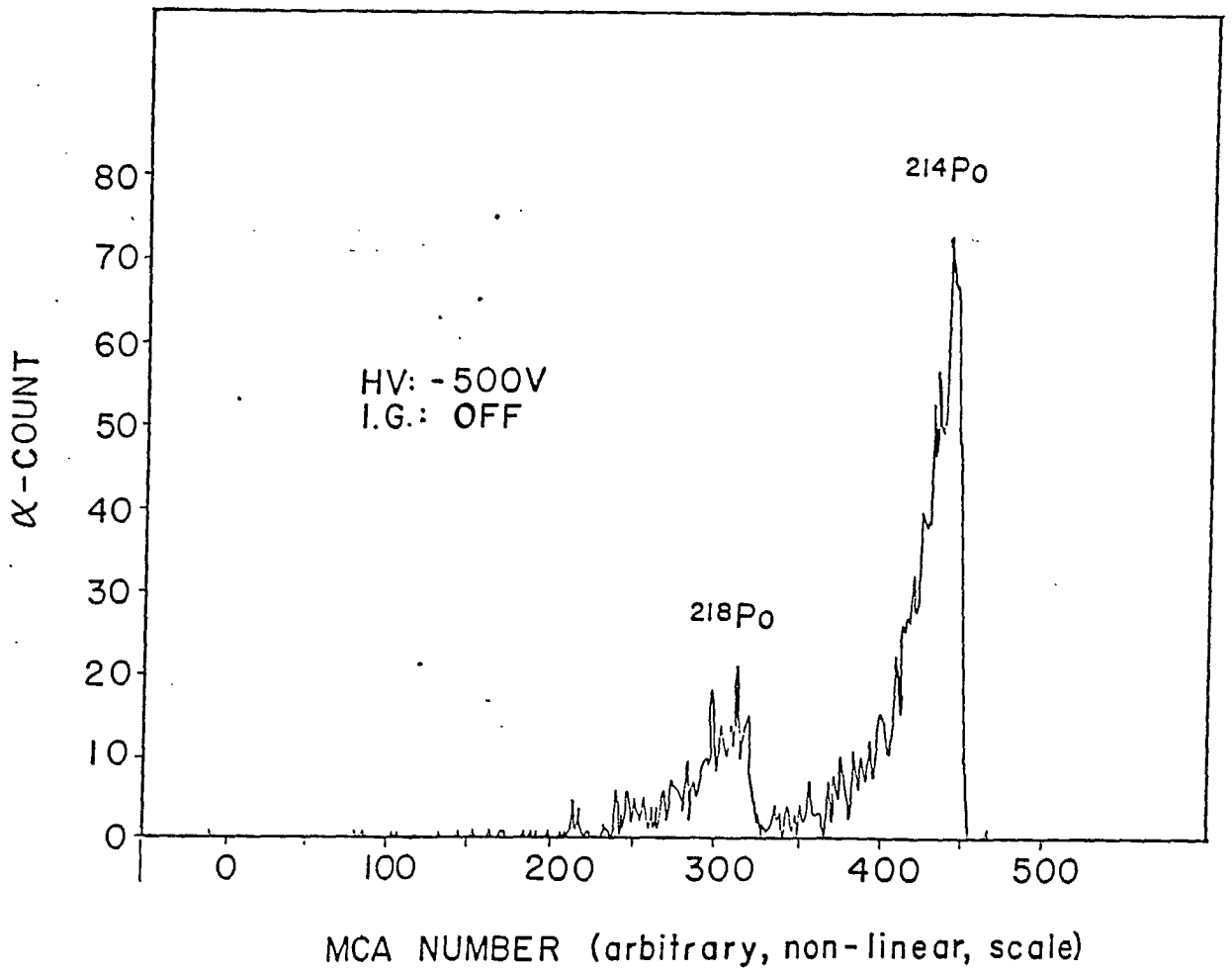

Fig. 5b - ^{222}Rn progeny spectrum (RTTF) for H.V. = -500 V.

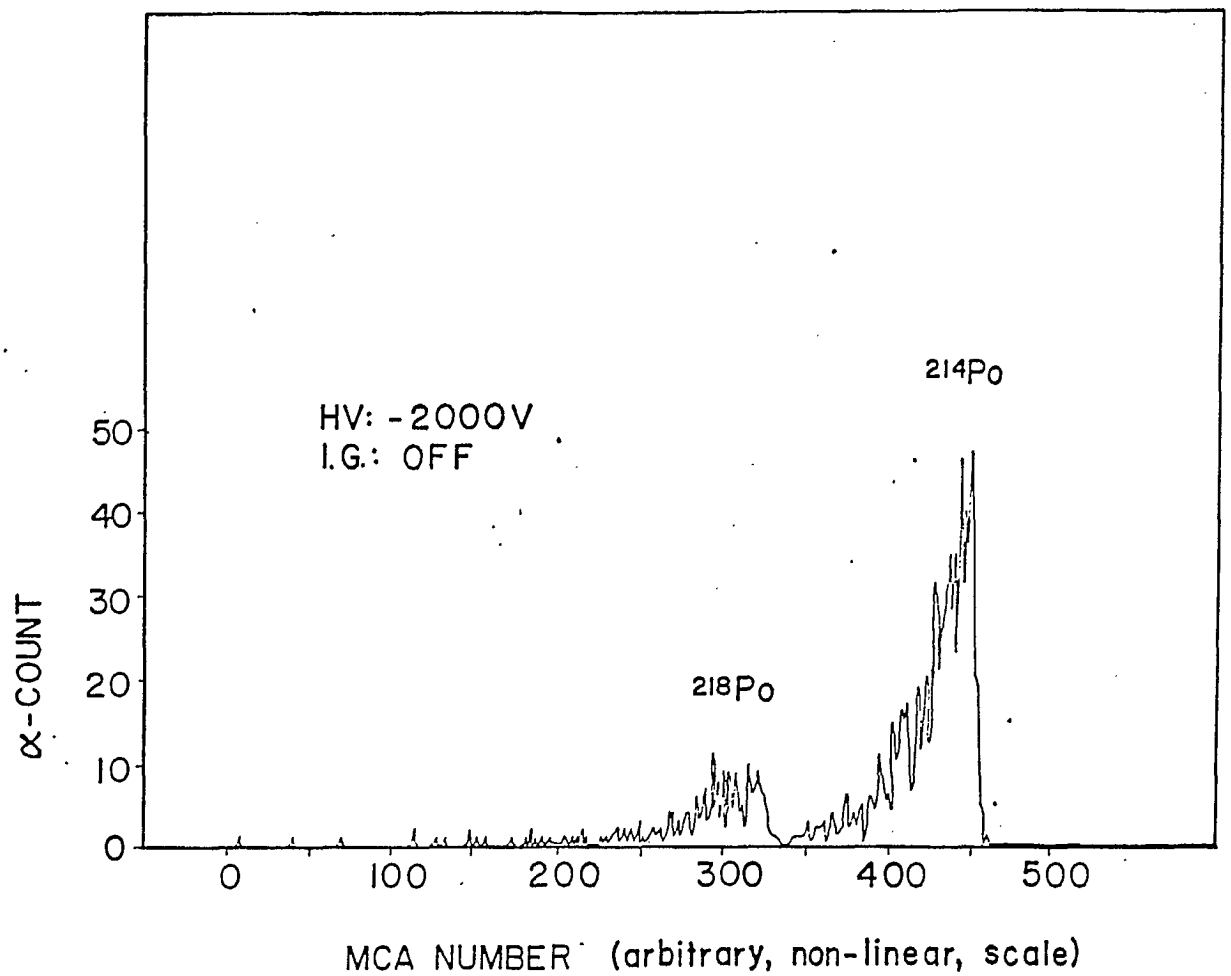

Fig. 5c - ^{222}Rn progeny spectrum (RTTF) for H.V. = -2000 V.

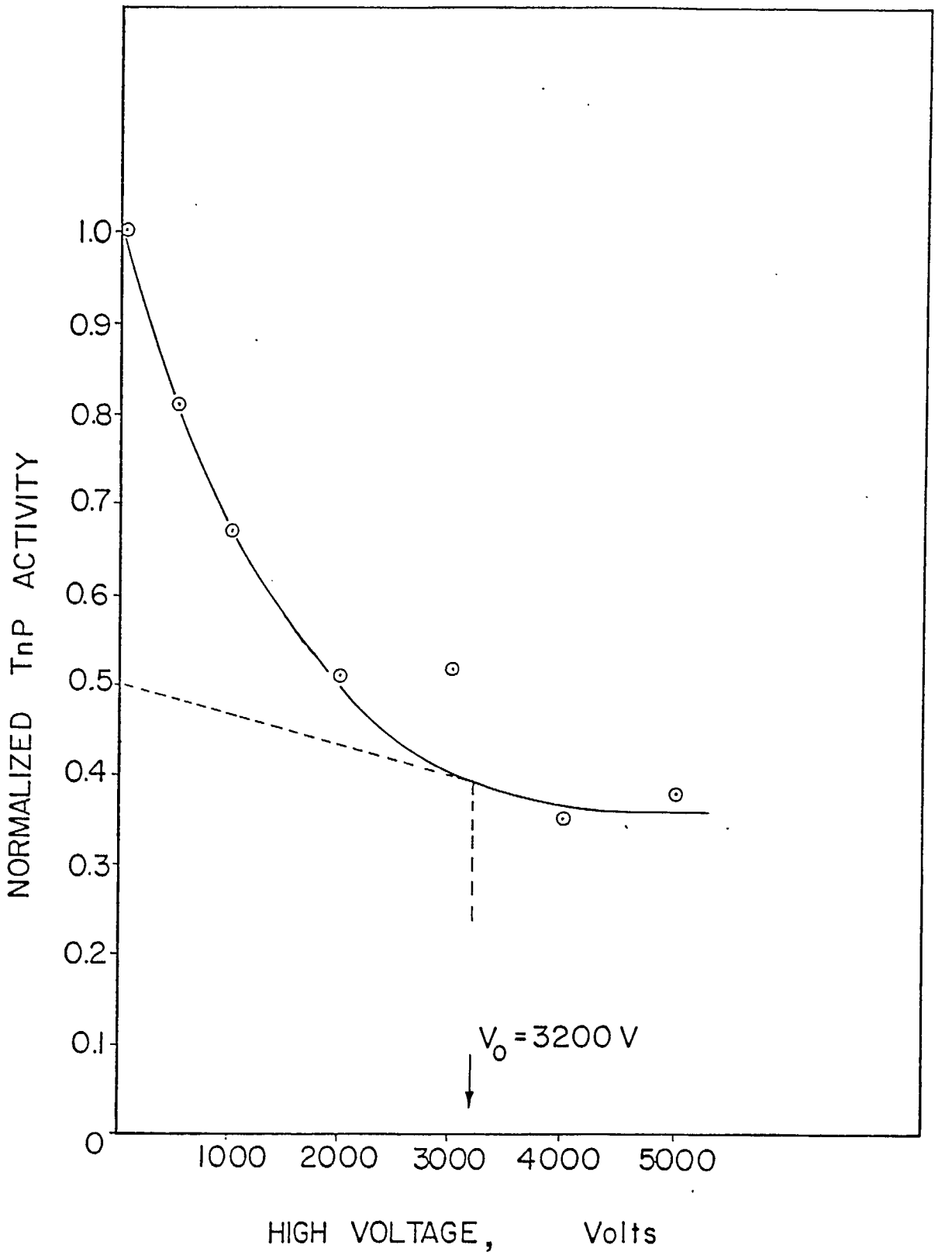

Fig. 6 - Normalized ^{220}Rn progeny (TnP) activity versus H.V. on the SFE.

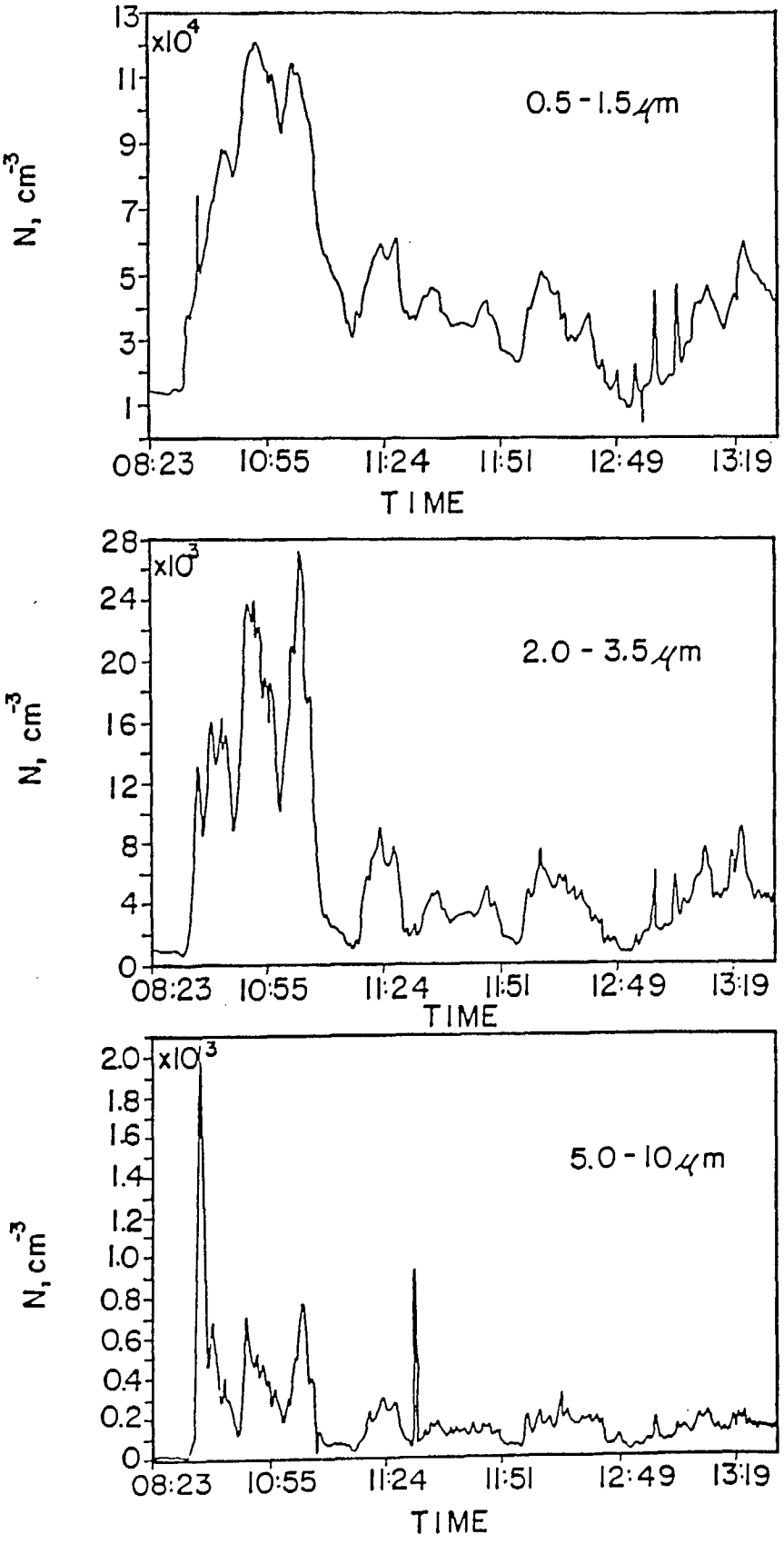

Fig. 7 - Dust size concentration versus time measured at the conveyor belt.

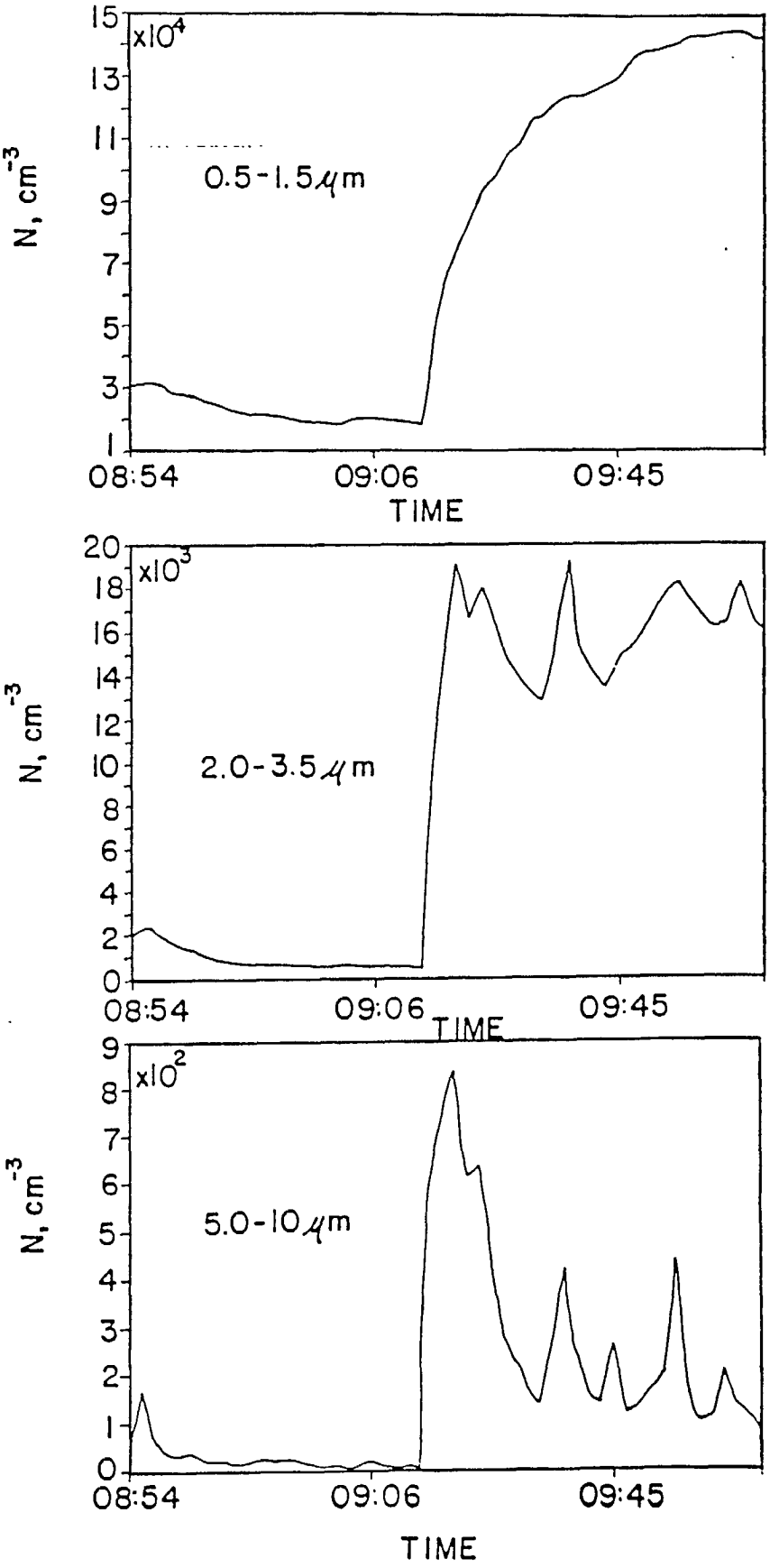

Fig. 8 - Dust size concentration versus time measured at the crusher platform.

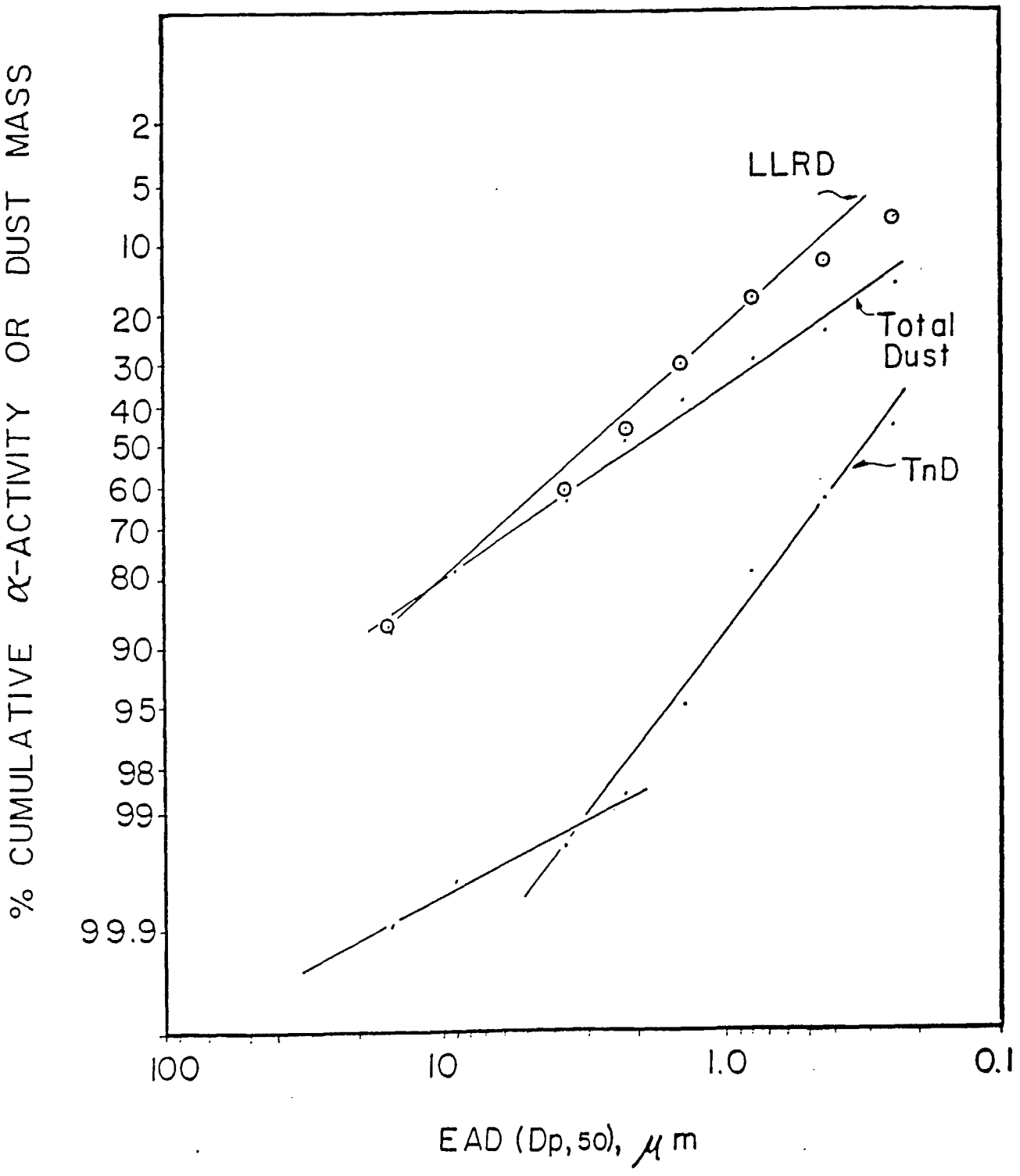

Fig. 9 - Percentage dust mass or α-particle activity versus EAD for LLRD, total dust, and ^{220}Rn progeny (TnD).

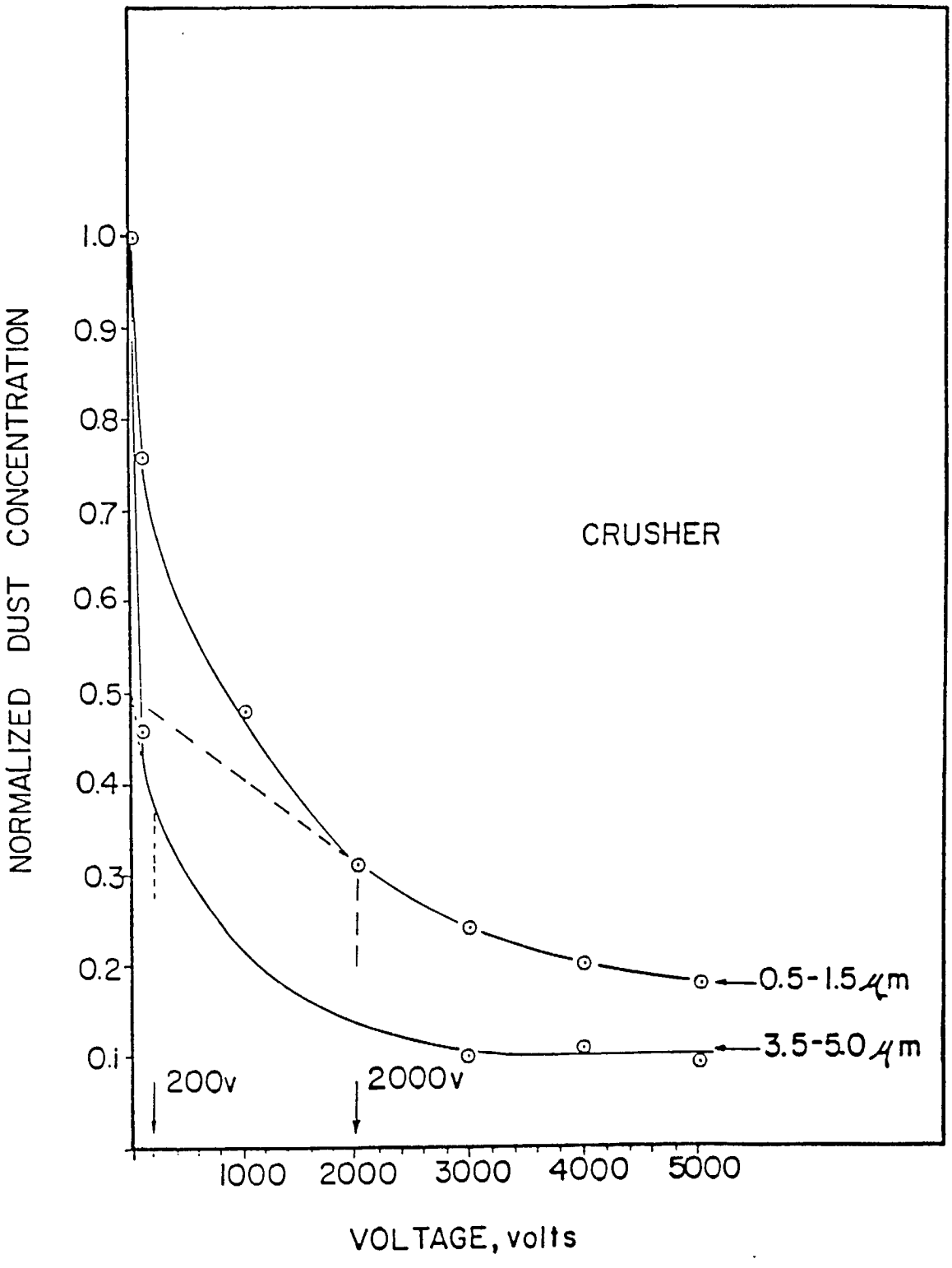

Fig. 10 - Normalized LLRD concentration (at the crusher) versus H.V. (on the SFE) for two different dust size ranges.

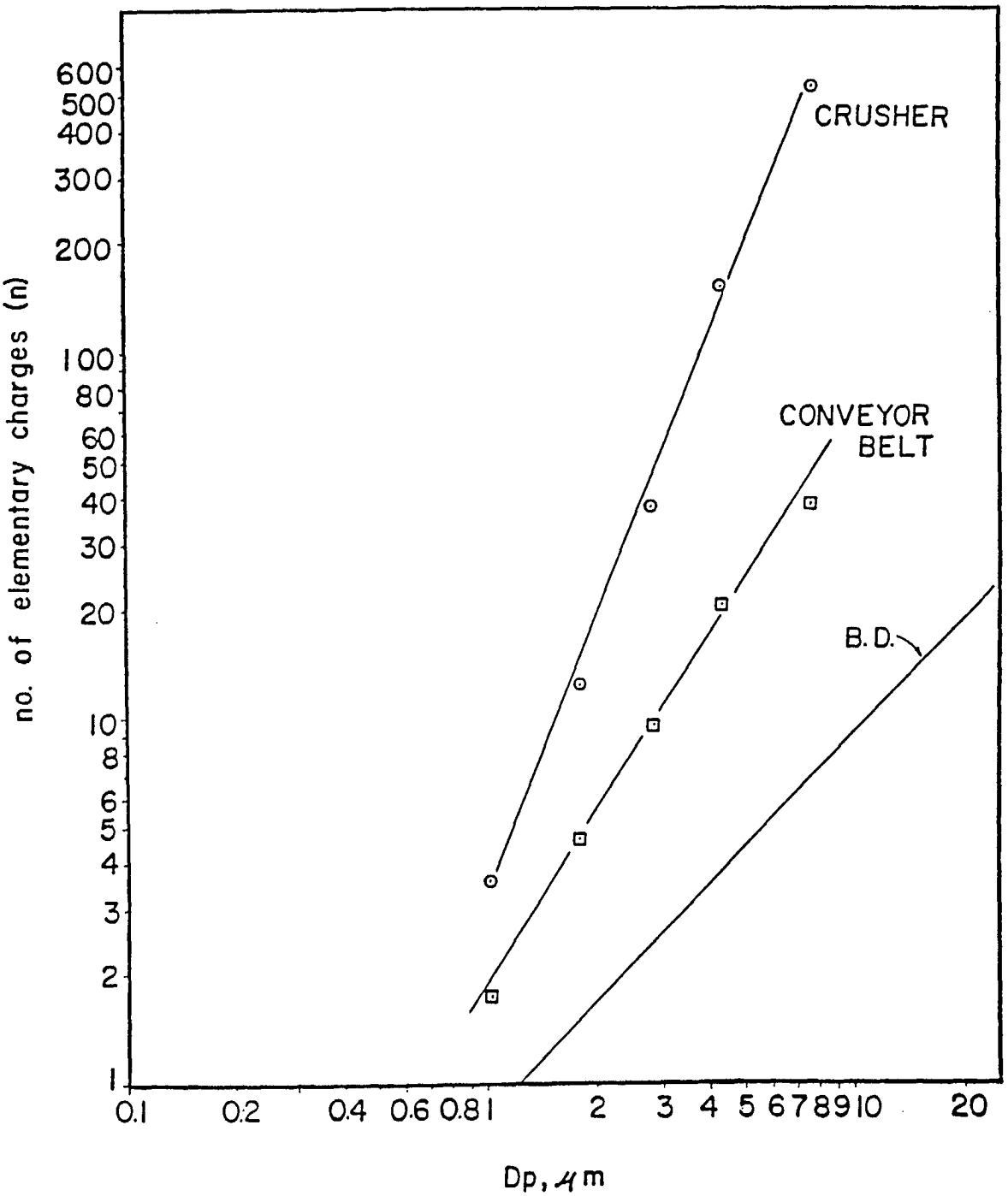

Fig. 11 - Electrical charge (n) versus particle size (Dp) for the crusher and the conveyor belt. Also shown is the Boltzmann's distribution (B.D.).